

Study on La-doped lithium-rich manganese-based cathode materials ($\text{Li}_{1.5}\text{Mn}_{0.7}\text{Co}_{0.15}\text{Ni}_{0.15}\text{O}_{2.5}$)

Zhongxiang Fu¹, Wei Li^{1,2,3,*}, Xiaotao Wang¹, Dehao Kong¹, Han Wu¹, Oimod Haschuluu^{1,2}, O. Tegus^{1,2,3}, Siqin Bator^{1,2}

¹ College of Physics and Electronic Information, Inner Mongolia Normal University, Hohhot 010022, Inner Mongolia, China;

² Inner Mongolia Key Laboratory for Physics and Chemistry of Functional Materials, Hohhot 010022, Inner Mongolia, China;

³ Inner Mongolia Engineering Research Center for Rare Earth Functional and New Energy Storage Materials, Hohhot 010022, Inner Mongolia, China

*E-mail: liweisyn@163.com

Received: 24 January 2022 / Accepted: 22 February 2022 / Published: 5 April 2022

The lithium-rich manganese-based cathode material $\text{Li}_{1.5}\text{Mn}_{0.7}\text{Co}_{0.15}\text{Ni}_{0.15}\text{O}_{2.5}$ was doped with La. The doping amounts were 0.1 wt%, 0.2 wt% and 0.3 wt%. X-ray diffraction (XRD) experiments show that the La-doped sample still maintains a layered structure, and no impurity phase is observed. Two-phase Rietveld full-spectrum refinement was performed on the samples before and after doping. The phase composition results show that the Li_2MnO_3 to $\text{LiNi}_{1/3}\text{Co}_{1/3}\text{Mn}_{1/3}\text{O}_2$ ratio of the synthesized material is 0.57:0.43, and La is doped in the Mn site of the Li_2MnO_3 phase. The charge–discharge test in the range of 2.0~4.5 V shows that the initial discharge specific capacity and the initial coulombic efficiency of the samples doped with 0.1 wt% and 0.2 wt% La are higher than those of the original samples. The initial discharge specific capacity after doping increases from 236.2 mAh/g to 251.5 mAh/g and 254.9 mAh/g. The initial coulombic efficiency after doping increases from 77.95% to 82.56% and 83.78%. La doping can obviously suppress the voltage decay of the material.

Keywords: La-doping modification; refinement; electrochemical performance

1. INTRODUCTION

The global energy sector is undergoing an unprecedented revolution. Because the massive consumption of fossil energy has exacerbated energy shortages and environmental crises and the environment is threatened, it is urgent to develop new energy sources to replace traditional energy sources such as coal, oil and natural gas. A chemical power source is an energy storage device with high energy conversion efficiency and environmental friendliness that has gradually entered people's daily lives. Lithium-ion batteries, as a chemical power source, have attracted much attention for their high energy and green characteristics. They have the advantages of high energy density, environmental

friendliness and long cycle life, which can continuously improve global demand. Since their commercialization in 1990, lithium-ion batteries have been widely used in portable electronic equipment. At the same time, they have shown broad application prospects and potential economic benefits in new energy vehicles and the defence industry. With the rapid development of new energy vehicles, higher requirements are proposed for the endurance mileage and other characteristics of power batteries. Cathode materials, as a key component of lithium-ion batteries, have a crucial influence on the electrochemical performance of batteries and affect battery energy density and capacity. In recent years, Li-rich manganese-based cathode materials composed of Li_2MnO_3 and LiMO_2 ($M = \text{Ni}, \text{Co}, \text{or Mn}$) have become one of the most promising cathode materials for lithium-ion batteries due to their discharge capacities being nearly twice those of traditional cathode materials (lithium cobaltite, lithium iron phosphate, lithium manganese oxide, etc.) [1-5]. After the first 4.5 V electrochemical activation, the material can activate anions (O^{2-}) to participate in the redox reaction and maintain a certain charge compensation ability in the subsequent cycle process. Lithium-rich manganese-based cathode materials show excellent electrochemical performance[6]. To ensure that anions participate in the redox reaction, the voltage window of lithium-rich manganese-based cathode materials needs to be expanded to 2–4.8 V. Such a high voltage will inevitably lead to a series of side reactions, such as serious initial oxygen loss side reactions at the interface between the electrolyte and material, and phase structure transformation. These side reactions will inevitably cause voltage attenuation and capacity loss[6]. Therefore, there are still many important problems to be solved for lithium-rich manganese-based materials at present, such as their low rate performance, high initial irreversible capacity and gradual decrease in the discharge plateau during cycling[7-10]. At the same time, the Li_2MnO_3 component has a lower Li^+ diffusion rate, which affects the rate performance of the material[8-10]. To solve these problems, materials need to be modified [11-14].

At present, the commonly used modification methods are surface-coating modification and doping modification. Although surface coating can reduce the extent of side reactions between the electrode material and electrolyte, it cannot guarantee the uniformity of the coating, which may damage the surface of the electrode material. [15]. Another method is doping, which uses other elements to replace oxygen atoms or transition metal atoms to stabilize the material structure and improve the electrochemical performance of the material. [16-18]. A large number of studies have shown that rare earth La doping can improve the charge–discharge capacity and cycle performance of lithium cobaltite, lithium manganate and lithium iron phosphate cathode materials[19-23]. In this paper, $\text{Li}_{1.5}\text{Mn}_{0.7}\text{Co}_{0.15}\text{Ni}_{0.15}\text{O}_{2.5}$ lithium-rich manganese-based cathode materials were doped with La. The effects of the La doping amount on the structure and electrochemical properties of lithium-rich manganese-based cathode materials were studied by using different doping amounts.

2. EXPERIMENT

2.1. Preparation of samples

$\text{NiSO}_4 \cdot 6\text{H}_2\text{O}$ (AR), $\text{CoSO}_4 \cdot 7\text{H}_2\text{O}$ (AR), $\text{MnSO}_4 \cdot \text{H}_2\text{O}$ (AR) and La_2O_3 were mixed into a solution with a certain concentration according to the stoichiometric ratio. The solution was introduced into ammonia with a peristaltic pump and stirred at high speed. The precursor was obtained after reaction,

filtration, washing and drying. The appropriate amount of precursor and Li_2CO_3 were mixed by grinding, and then, the resulting material was sintered at high temperature. The sintering temperature was $850\text{ }^\circ\text{C}$, and the holding time was 8 hours. Finally, cathode materials doped with 0%, 0.1%, 0.2%, and 0.3% La were synthesized. In the following, LMO is used to represent $\text{Li}_{1.5}\text{Mn}_{0.7}\text{Co}_{0.15}\text{Ni}_{0.15}\text{O}_{2.5}$.

2.2. Material structure and morphology characterization

The crystal structure of the material was analysed by X-ray diffraction (XRD), and the test was carried out with a Panaco Empyrean sharp shadow X-ray diffractometer. The scanning range was $10^\circ\sim 90^\circ$, and the step length was 0.01° (Cu $K\alpha$ radiation, $\lambda=0.154184\text{ nm}$, 40 kV tube voltage, 40 mA tube current). The surface morphology of these samples was observed by a Hitachi SU8010 scanning electron microscope.

2.3. Electrochemical performance test

The cathode electrode sheet was prepared as follows: the cathode material, polyvinylidene fluoride (PVDF) and conductive agent (acetylene black, conductive graphite) were mixed evenly by stirring according to a mass ratio of 8:1:1 using N-methyl pyrrolidone (NMP) as a dispersant, and then, the mixture was uniformly coated on aluminium foil. The battery was assembled in a glove box protected by argon gas with a water content and oxygen content of less than 0.1 ppm. The battery assembly order was negative shell, negative material, diaphragm, electrolyte, positive material, steel sheet, spring, and battery positive shell. The assembled battery model was a LIR2032 button battery. The battery used a lithium sheet as the negative electrode and a microporous polypropylene film as the diaphragm. In this experiment, a LAND (CT2001A) battery tester was used to conduct a constant-current charge–discharge test on the assembled button battery, and the test voltage range was 2.0–4.5 V. The impedance of the assembled button battery was tested by a CHI660E electrochemical workstation.

3. RESULTS AND DISCUSSION

3.1. XRD measurements

Figure 1 (a) shows the XRD patterns of Li-rich manganese-based layered cathode materials doped with different La contents. The diffraction pattern shows that the diffraction patterns before and after doping are basically the same and that no impurity is found. The diffraction peaks of the four groups of samples are basically consistent with the layered structure of $\alpha\text{-NaFeO}_2$ and belong to the R-3m space group. There is a weak diffraction peak at $20\text{-}25\text{ }^\circ\text{C}$ corresponding to the Li_2MnO_3 component according to phase retrieval. The splitting of diffraction peaks at $(006)/(012)$ and $(018)/(110)$ indicated that the material had an obvious layered structure. No impurity peaks were found in the spectra, indicating that the structure did not change significantly after La doping [24]. Figure 1 (b) shows the local amplification of (003). The figure shows that the entire pattern of the sample doped with La shifts to the

left. According to the elemental ion radius, the radius of La^{3+} (10.4 nm) was larger than the radii of Ni^{2+} (6.9 nm), Mn^{4+} (5.3 nm) and Co^{2+} (7.45 nm)[25], which caused the leftward shift of the doped peak. This indicates that La entered the material lattice and achieved bulk doping.

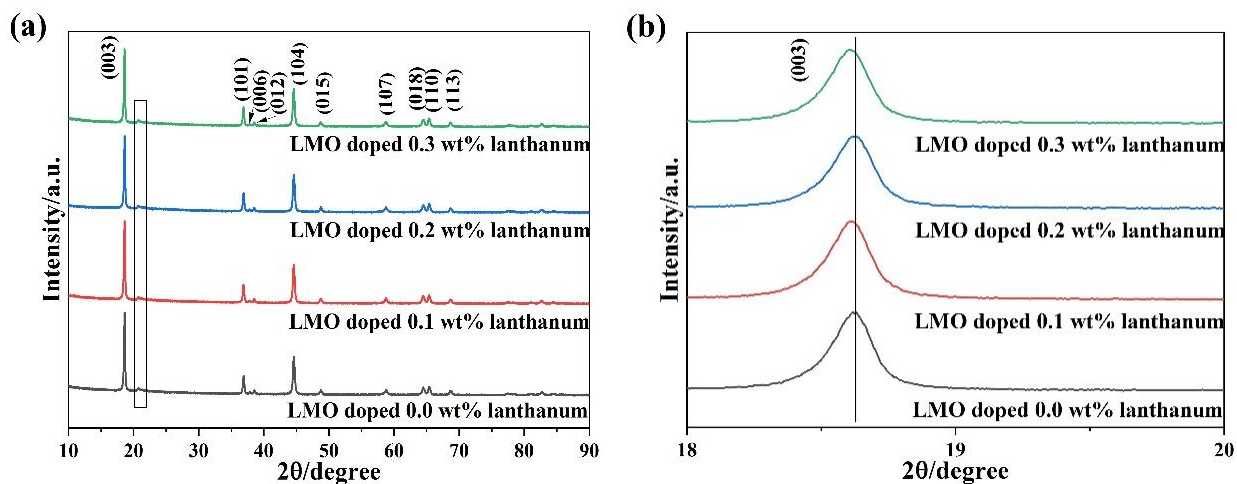


Figure 1. XRD patterns of (a) lithium-rich manganese-based cathode materials doped with different La contents and (b) a partially enlarged view of the (003) peak. Test angle: 10° - 90° ; step size: 0.01° .

The XRD patterns show that the main diffraction peaks of the samples before and after doping can be attributed to the R-3m space group. There is a weak diffraction peak at 20-25 °C, and the composition of Li_2MnO_3 corresponding to the C2/m space group was determined by phase retrieval. This is due to the ordered arrangement of Li and Mn in the transition metal layer forming a honeycomb superlattice structure[25]. The ratio of Li_2MnO_3 to LiMO_2 ($\text{M} = \text{Ni}_{1/3}\text{Co}_{1/3}\text{Mn}_{1/3}$) affects the charge capacity of Li-rich Mn-based materials[26]. Therefore, to clarify the ratio of the Li_2MnO_3 phase to the $\text{LiNi}_{1/3}\text{Co}_{1/3}\text{Mn}_{1/3}\text{O}_2$ phase in the synthesized material, R-3m and C2/m two-phase refinement of undoped samples was carried out. The structural model constructed according to the atomic coordinates and atomic occupation information of the undoped sample is shown in Figure 2. Table 1 and Table 2 show the two-phase atomic position and atomic occupation information. It can be concluded that there are four Mn atoms, eight Li atoms and twelve O atoms in the synthesized Li_2MnO_3 phase and three Li atoms, one Mn atom, one Ni atom, one Co atom and six O atoms in the $\text{LiNi}_{1/3}\text{Co}_{1/3}\text{Mn}_{1/3}\text{O}_2$ phase of the synthesized material. According to the atomic number, the ratio of the Li_2MnO_3 phase to the $\text{LiNi}_{1/3}\text{Co}_{1/3}\text{Mn}_{1/3}\text{O}_2$ phase in the actual synthesized material is 0.57:0.43. Therefore, the synthesized material is 0.57 Li_2MnO_3 -0.43 $\text{LiNi}_{1/3}\text{Co}_{1/3}\text{Mn}_{1/3}\text{O}_2$ ($\text{Li}_{1.5}\text{Mn}_{0.7}\text{Co}_{0.15}\text{Ni}_{0.15}\text{O}_{2.5}$).

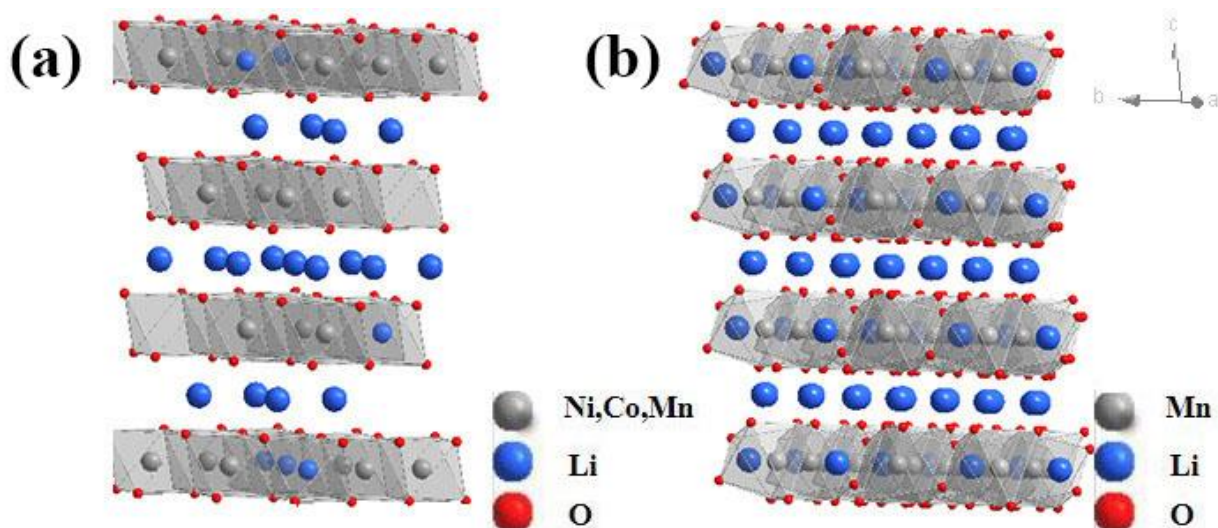


Figure 2. Two-phase structure model of undoped samples: (a) $\text{LiNi}_{1/3}\text{Co}_{1/3}\text{Mn}_{1/3}\text{O}_2$ phase structure model and (b) Li_2MnO_3 phase structure model.

Table 1. $\text{LiNi}_{1/3}\text{Co}_{1/3}\text{Mn}_{1/3}\text{O}_2$ atomic coordinates and occupancy information.

Atom	Site	x	y	z	Occupancy
O1	6c	0	0	0.24157	0.173
Co1	3b	0	0	0.5	0.027
Ni2	3a	0	0	0	0.002
Mn1	3b	0	0	0.5	0.028
Ni1	3b	0	0	0.5	0.026
Li2	3b	0	0	0.5	0.002
Li1	3a	0	0	0	0.081

Table 2. Li_2MnO_3 atomic coordinates and occupancy information.

Atom	Site	x	y	z	Occupancy
Mn1	4g	0	0.22912	0	0.492
Li1	2b	0	0.5	0	0.24
Li2	2c	0	0	0.5	0.213
Li3	4h	0	0.805	0.5	0.864
O1	4i	0.17545	0	0.16039	0.507
O2	8j	0.35905	0.34126	0.28921	1.12

To determine which phase is replaced by La, the samples doped with 0.3% La were two-phase refined. La doping (0.3%) was performed on the two-phase manganese sites of the samples. The results are shown in Figure 3. Figure 3 (a) shows the structure refinement diagram of La-doped $\text{LiNi}_{1/3}\text{Co}_{1/3}\text{Mn}_{1/3}\text{O}_2$, and Figure 3 (b) shows the structure refinement diagram of La-doped Li_2MnO_3 . Table 3 shows the bond length information of the doped two-phase La-O bond. The shorter the bond length is, the more stable the structure. The table shows that the La-O bond formed when La replaced Mn in the Li_2MnO_3 phase is the shortest, and the structure is more stable than the $\text{LiNi}_{1/3}\text{Co}_{1/3}\text{Mn}_{1/3}\text{O}_2$ phase. This shows that La is in the Li_2MnO_3 phase after doping.

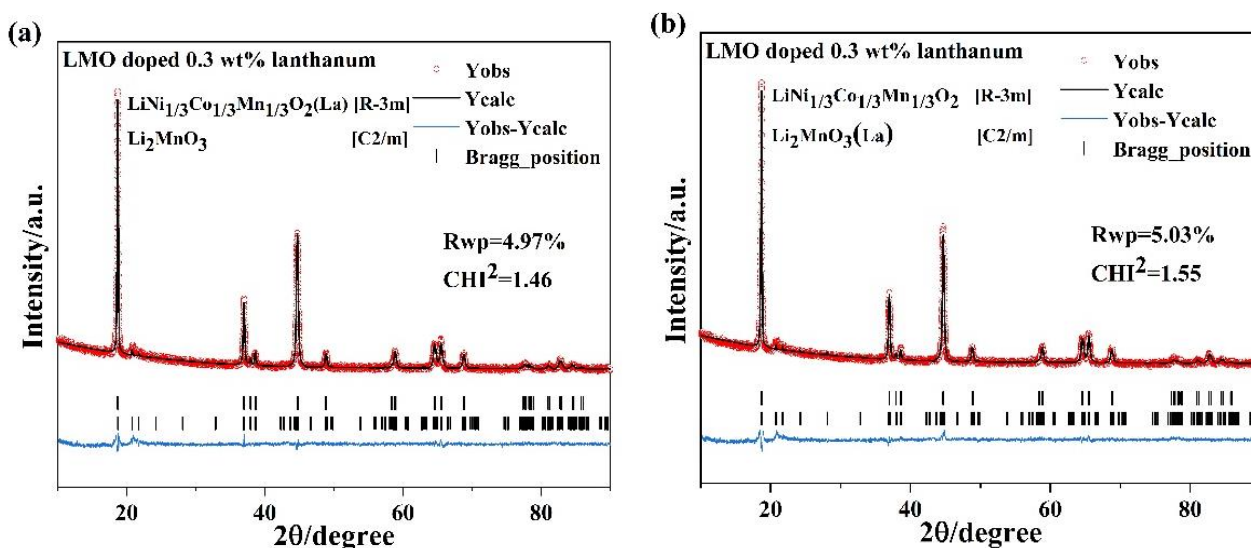


Figure 3. (a) Refined graph of the La-doped $\text{LiNi}_{1/3}\text{Co}_{1/3}\text{Mn}_{1/3}\text{O}_2$ phase. (b) Refined graph of the La-doped Li_2MnO_3 phase.

Table 3. La-O bond length information of the La-doped $\text{LiNi}_{1/3}\text{Co}_{1/3}\text{Mn}_{1/3}\text{O}_2$ and Li_2MnO_3 phases.

Interatomic distances/nm	$\text{LiNi}_{1/3}\text{Co}_{1/3}\text{Mn}_{1/3}\text{O}_2$	Li_2MnO_3
La-O average	0.45642	0.392

Figure 4 shows the two-phase refinement diagram before and after doping, and Table 4 shows the XRD refinement data before and after doping. Since La is doped in the Li_2MnO_3 phase, the cell information of the Li_2MnO_3 phase is analysed. In Table 4, *a* reflects the distance between adjacent metal ions in the transition metal layer, and *c* reflects the spacing of lithium layers [27]. *a* and *c* can be effectively increased in Li_2MnO_3 , which increases the cell volume. However, due to too low of a doping amount, the increase is not obvious. Therefore, La enters the crystal structure of the Li-rich Mn-based cathode material and expands its cell [28]. In the refined figure, *Rwp* is the reliability factor, and CHI^2 is the goodness of fit. In all the refined maps in this paper, *Rwp* is less than 10%, and CHI^2 is less than 2. This conforms to the reliable judgement standard of refined results [29]. This also shows that La is indeed doped in the Mn site of the Li_2MnO_3 phase.

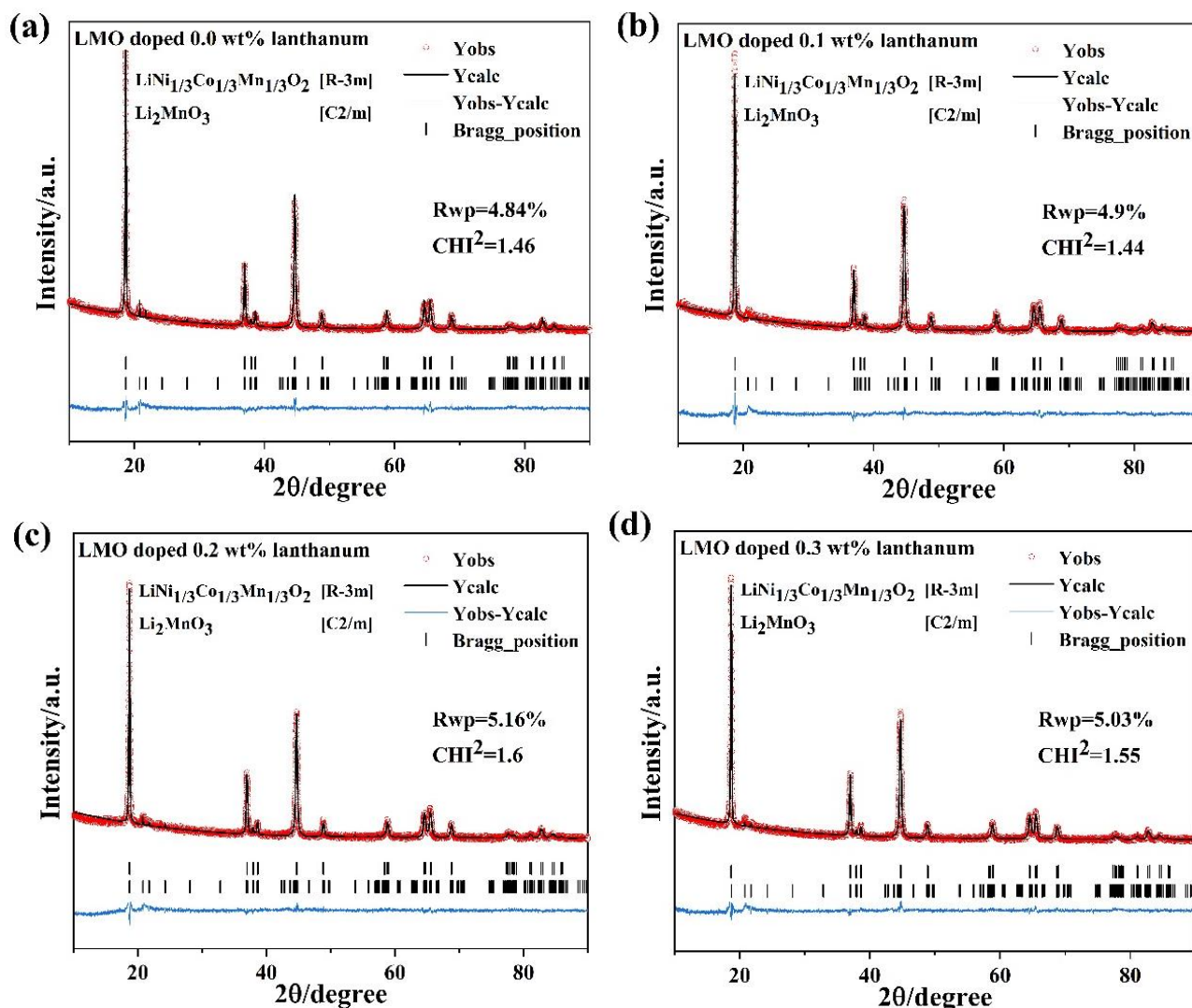


Figure 4. XRD refinement graph of the (a) undoped sample, (b) sample doped with 0.1% La, (c) sample doped with 0.2% La, and (d) sample doped with 0.3% La.

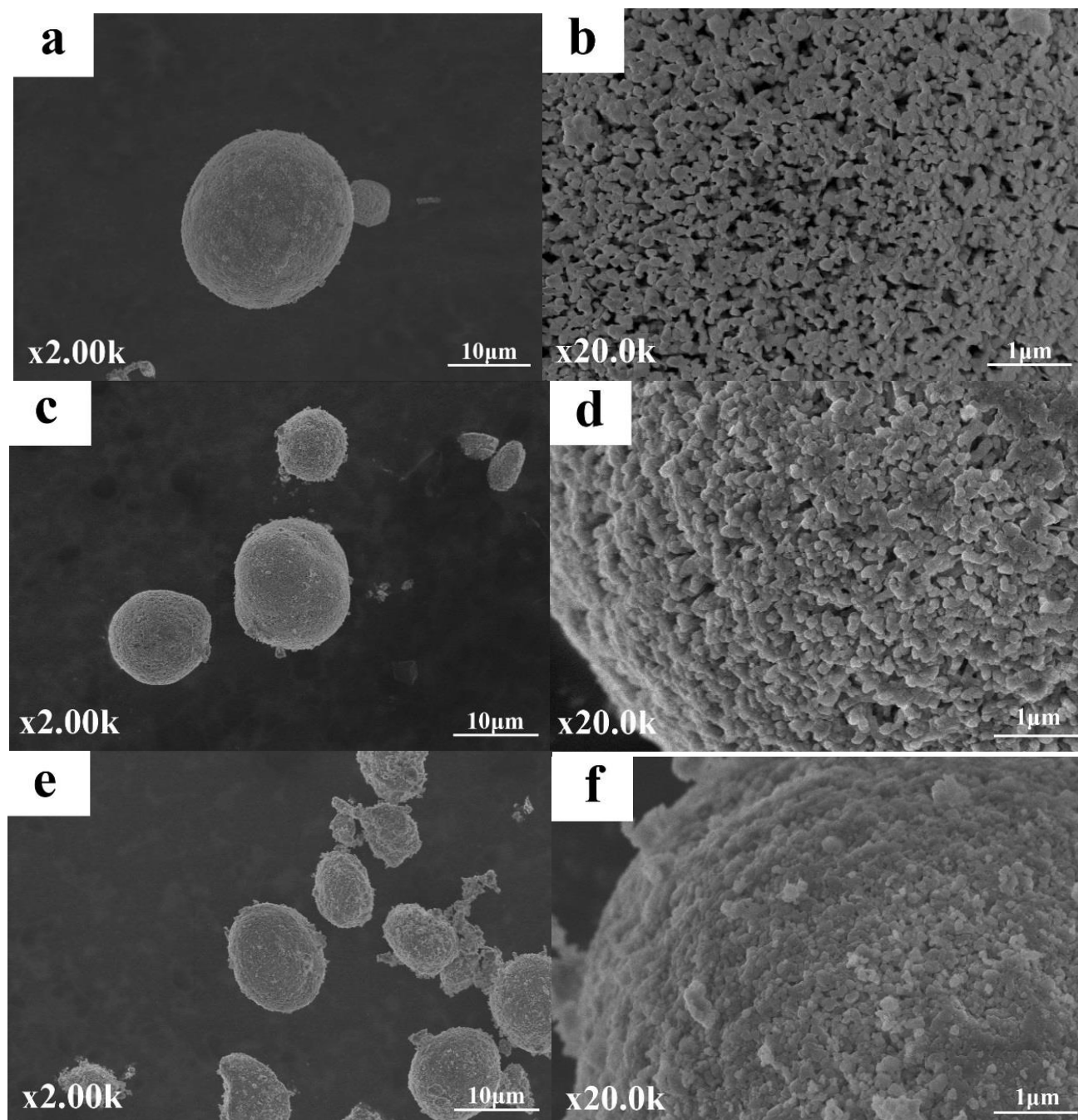
Table 4. Refined crystal parameters of samples doped with different La contents (R-3m space group).

Doping content/%	a/nm	c/nm	V/nm ³
0	0.28481	1.42301	0.099972
0.1	0.28483	1.42289	0.098979
0.2	0.28485	1.42294	0.099992
0.3	0.28486	1.42317	0.100015

3.2. Analysis of the electrode material morphology

Figure 5 shows scanning electron microscopy (SEM) images of the samples before and after doping. The figure shows that the sintered sample is still spherical, and only part of the sphere is broken. As shown in Figure 5(b), there are dense pores on the surface of the undoped sample. This may be due

to the release of gas during sintering. The pore size of the doped samples decreases obviously, which is beneficial to the stability of the structure. When the doping amounts were 0.2% and 0.3%, a small amount of small particles adhered to the sample surface, which may be because La did not completely enter the lattice and thus affected the electrochemical performance.



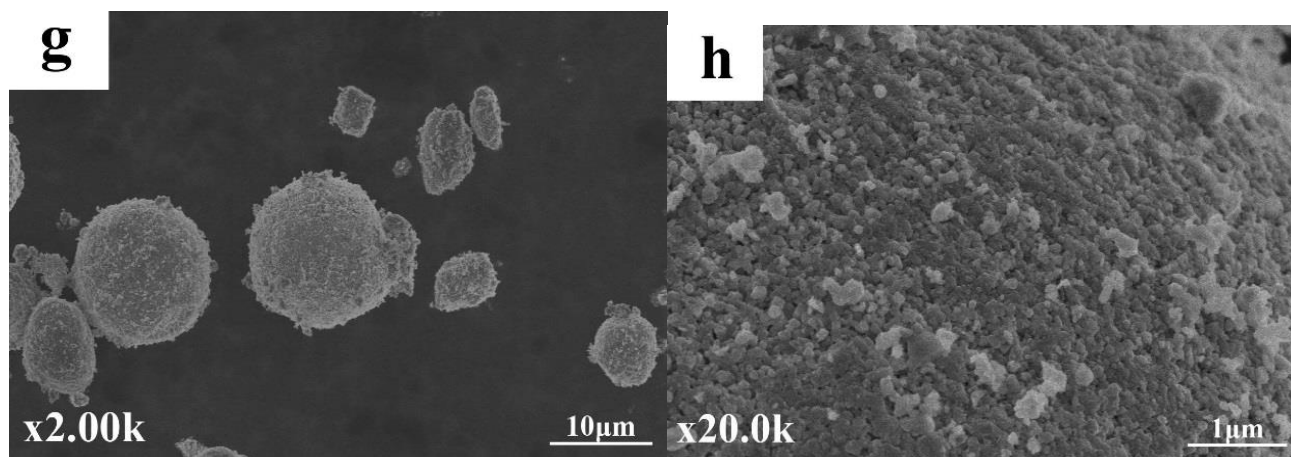


Figure 5. SEM images of the (a)-(b) undoped sample, (c)-(d) sample doped with 0.1% La, (e)-(f) sample doped with 0.2% La, and (g)-(h) sample doped with 0.3% La.

3.3. Electrochemical performance analysis

The four groups of samples were electrochemically tested at room temperature in the voltage range of 2.0~4.5 V. The initial charge–discharge curves and electrochemical data of lithium-rich manganese layered cathode materials doped with different La contents at 0.2 C are shown in Figure 6 and Table 5. Figure 5 shows that the charge–discharge curves of the four groups of samples are consistent. The slope area below 4.5 V of the charge curve represents the oxidation process of Ni^{2+} and Co^{3+} , and the L-shaped plateau above 4.5 V represents the oxidation process of O^{2-} . This process is also accompanied by the release of lithium ions and the activation of Li_2MnO_3 [30-32]. The initial discharge capacity reaches a maximum of 254.9 mAh/g when the doping amount is 0.2%. Table 5 shows that the irreversible specific capacity decreases from 66.8 mAh/g to 53.1 mAh/g and 49.3 mAh/g compared with that of the undoped samples when the doping amounts are 0.1% and 0.2%, respectively, and the initial charge–discharge coulombic efficiency increases from 77.95% to 82.56% and 83.78%, respectively. This may be because a small La doping amount can not only broaden the lithium ion transport channel but also effectively allow La to enter the lattice to enhance the bond interaction between O and the metal layer, which improves the material capacity and the initial reversible efficiency. However, when the doping amount is 0.3%, the initial discharge capacity is only 200.2 mAh/g, and the initial charge–discharge coulombic efficiency is only 65.33%. When the doping amount is 0.3%, the inability of La to fully enter the material lattice hinders the transmission of lithium ions, thereby deteriorating the initial discharge capacity and the initial coulombic efficiency of the material. The diagram shows that the undoped sample and the sample doped with 0.3% La exhibit charging voltage hysteresis, which may lead to voltage attenuation, and there is a plateau at 2 V, which may be caused by the change in structural position[33].

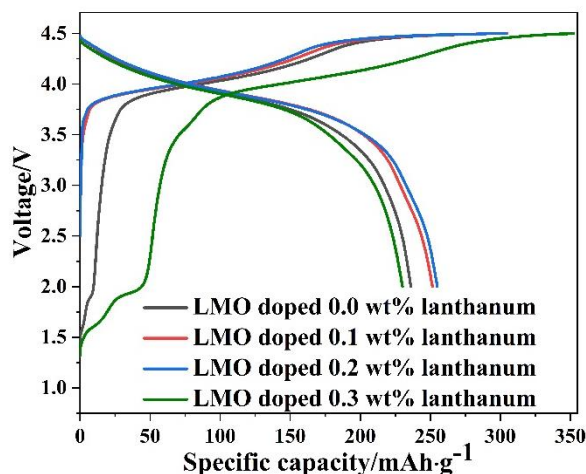


Figure 6. Initial galvanostatic charge/discharge curves of samples doped with different La contents at 0.2 C between 2.0 and 4.5 V using Li metal as the anode.

Table 5. Initial cycle charge and discharge data of these materials.

Doping content /%	Initial charge specific capacity/(mAh·g ⁻¹)	Initial discharge specific capacity/(mAh·g ⁻¹)	Irreversible specific capacity/(mAh·g ⁻¹)	Initial t charge and discharge efficiency/%
0	303	236.2	66.8	77.95
0.1	304.6	251.5	53.1	82.56
0.2	304.2	254.9	49.3	83.78
0.3	352.4	230.2	122.2	65.33

Figure 7(a) shows the AC impedance diagram and equivalent circuit diagram of the samples doped with different contents of La. The assembled batteries were activated at a current density of 0.2 C at 2~4.5 V, and then, impedance measurements were performed at 0.005 V and 1-10⁵ Hz using a CHI660e electrochemical workstation. The four sets of data consist of the semicircle in the high-frequency region and the slash in the low-frequency region. In the equivalent circuit, R_s represents the conduction impedance of lithium ions passing through the SEI film in the high-frequency region, R_{ct} represents the charge transfer impedance, and the slope line in the low-frequency region linked to the Warburg impedance (Z_w) refers to the process of Li diffusion in the bulk lattice [34-35]. As the doping amount increases, R_{ct} gradually decreases, indicating that a greater amount of doped La is conducive to charge transfer. However, when the doping amount is 0.2%, R_s reaches the minimum and is reduced from 3.586 Ω to 3.515 Ω compared with that of the original sample. This indicates that a doping amount of 0.2% is beneficial for lithium ions to pass through the SEI film, which may be the reason for the high initial discharge specific capacity[36]. The sample doped with 0.1% La has the lowest R_{ct} because doped La occupies part of the Mn sites in the Li₂MnO₃ phase, resulting in partial Mn stripping, hindering the Li⁺ transmission channel and increasing R_{ct} . With the increase in the doping amount, the Li⁺

transmission channel becomes wider, resulting in a decrease in R_{ct} . To study the lithium-ion transmission ability, the lithium-ion diffusion coefficient (D_{Li^+}) is explored, and the formula is as follows:

$$D_{Li^+} = R^2 T^2 / 2 A^2 n^4 F^4 c^2 \sigma^2 \tag{1}$$

$$Z' = \sigma \omega^{-1/2} \tag{2}$$

where Z' is the Warburg impedance, σ is the Warburg impedance factor, ω is the angular frequency, R is the gas constant, T is the experimental environment temperature, A is the area of the cathode material immersed in the electrolyte, n is the number of electrochemical reaction electrons, F is the Faraday constant, and c is the lithium-ion concentration [37-38].

The slope of the line in the low-frequency region reflects the Warburg impedance, which is related to the diffusion process of lithium ions in bulk materials [39,40]. The relationship between Z' and $\omega^{-1/2}$ in the low-frequency region of the four groups of samples and the fitting results are shown in Figure 7(b). The lithium-ion diffusion coefficient can be qualitatively estimated by the slope of the straight line. Obviously, the lithium-ion diffusion coefficient of the sample doped with 0.3% is the largest. The results show that the sample doped with 0.3% La has a higher Li^+ transfer rate.

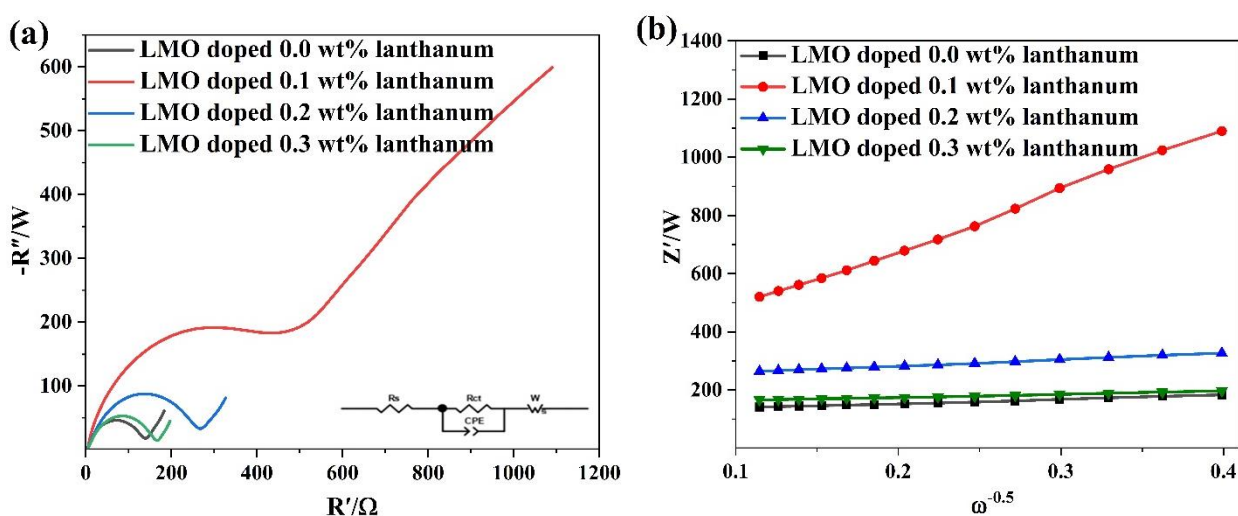


Figure 7. (a) Electrochemical impedance spectra of activated lithium-rich manganese-based cathode materials doped with different La contents at 0.005 V and $1-10^5$ Hz using a CHI660e electrochemical workstation and (b) Z' to $\omega^{-0.5}$ linear relationship diagram.

Table 6. Impedance fitting values of samples after activation.

Doping content/%	R_s/Ω	R_{ct}/Ω
0	3.586	126.5
0.1	3.743	410.3
0.2	3.515	267.3
0.3	4.86	160.2

Figure 8 shows the cycle performance diagram of lithium-rich manganese-based cathode materials doped with different contents of La after 100 cycles. The diagram shows that the cycle

performance of the sample doped with 0.1% La is the worst, and the discharge capacity is only 184.2 mAh/g after 100 cycles at a rate of 0.6 C. This is because the charge transfer impedance of the sample doped with 0.1% La is the largest, and the lithium ion transmission capacity is the worst, which affects the lithium ion intercalation process. With increasing doping amount, R_{ct} decreases, which promotes the transfer of Li^+ and improves the cycling stability. The sample doped with 0.3% La has the best cycle stability among the three groups of data after doping. At a rate of 0.6 C, the discharge capacity after 100 cycles is 217.4 mAh/g, which is greater than that of the sample doped with 0.2% and consistent with the impedance fitting results.

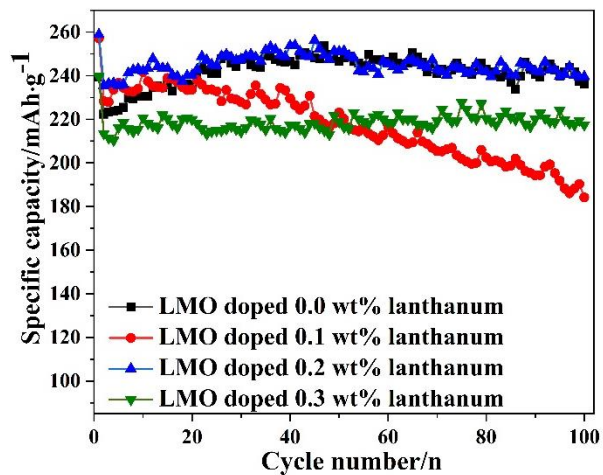


Figure 8. Cycle performance of lithium-rich manganese-based cathode materials doped with different La contents at 0.6 C and between 2.0 and 4.5 V using Li metal as the anode.

Figure 9 is the median voltage curve of the sample cycled 50 times. The figure shows that the voltage decay of the doped sample is slower than that of the undoped sample. The sample doped with 0.3% La has the highest initial median voltage. In the first cycle, the median voltages of the samples before and after doping are 3.8719 V, 3.8702 V, 3.9036 V, and 3.8493 V. After 50 cycles, the median voltages are attenuated to 3.6176 V, 3.6376 V, 3.66 V, and 3.6095 V. The voltage decay of undoped and 0.3% doped samples is the fastest, which is related to the voltage hysteresis of the first charge curve. This indicates that doping with an appropriate amount of La can effectively maintain the median voltage, effectively stabilize the material structure when La enters the matrix material lattice, and avoid the transition of the layered structure to the spinel structure during cycling so that the material maintains a high median voltage and a slow attenuation trend, which is beneficial to improve the electrochemical performance of the material.

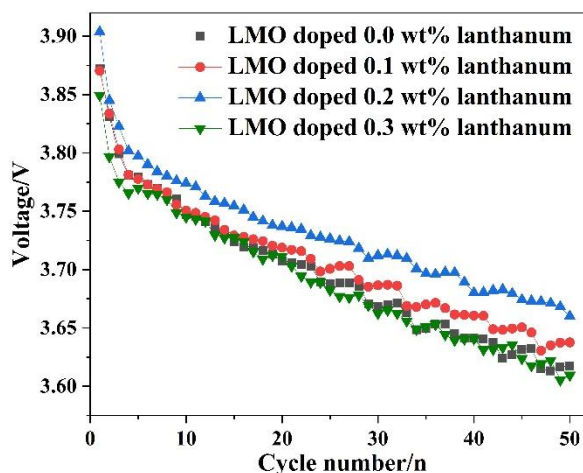


Figure 9. Median voltage curve of lithium-rich manganese-based cathode materials doped with different La contents at 0.6 C and between 2.0 and 4.5 V using Li metal as the anode.

4. CONCLUSIONS

In the solid-state synthesis method, doping with a small amount of lanthanum does not affect the layered structure of $\text{Li}_{1.5}\text{Mn}_{0.7}\text{Co}_{0.15}\text{Ni}_{0.15}\text{O}_{2.5}$. The phase composition results show that the Li_2MnO_3 to $\text{LiNi}_{1/3}\text{Co}_{1/3}\text{Mn}_{1/3}\text{O}_2$ ratio of the synthesized material is 0.57:0.43. La doped in the Mn site of the Li_2MnO_3 phase. The initial discharge capacity and coulombic efficiency can be improved by doping with an appropriate amount of La. Due to the small doping amount, the improvement in cycle stability is not ideal but has shown great potential. Doping with La can alleviate voltage attenuation and effectively avoid the transformation of the layered structure to the spinel structure during cycling.

ACKNOWLEDGMENT

This work was financially supported by the National Natural Science Foundation of China (No. 21865021), the Inner Mongolia Key Technology Project (No. 2020GG0166) and the High-level Scientific Research Foundation for the Introduction of Talent of Inner Mongolia Normal University (No. 2018YJRC019).

References

1. M. Hu, X.L. Pang, Z. Zhou., *J. Power source*, 237 (2013) 229.
2. L.J. Ma, J.Q. Meng, Y. Pan, Y.J. Cheng, Q. Ji, X.X. Zuo, X.Y. Wang, J. Zhu, Y.J. Xia, *Langmuir*, 36 (2020) 2003.
3. G.R. Hu, Z.C. Xue, Z.Y. Luo, Z.D. Peng, Y.B. Cao, W.G. Wang, Y.X. Zeng, Y. Huang, T.F. Li, Z.Y. Zhang, K. Du, *Ceram.int.*, 45(8) (2019) 10633.
4. Z.G. Tai, W. Zhu, M. Shi, Y.F. Xin, S.W. Guo, Y.F. Wu, Y.F. Chen, Y.N. Liu, *J. Colloid Interface Sci.*, 576 (2020) 468.
5. D. Mohanty, S. Kalnaus, R.A. Meisne, K.J. Rhodes, J.L. Li, E.A. Payzant, D.L. Wood, C. Daniel, *J. Power Sources*, 229 (2013) 239.
6. M.M. Geng, K. Yang, H.X. Mao, Y.X. Gao, J.J. Zhong, *Rare Met. Cemented Carbides*,

- 48 (2020) 61.
7. E.Y. Zhao, X.Q. Yu, F.W. Wang, H. Li, *Sci. China Chem.*, 60 (12) (2017) 1483.
 8. Y. Wu, A. Manthiram, *Solid State Ionics*, 180 (2009) 50.
 9. Q.Y. Wang, J. Liu, A.V. Murugan, A. Manthiram, *J. Mater. Chem. A*, 19 (28) (2009) 4965.
 10. W. He, J.F. Qian, Y.L. Cao, X.P. Ai, H.X. Yang, *RSC Adv.*, 2 (2012) 3423.
 11. J.H. Gao, T. Yuan, S.N. Luo, J.F. Ruan, H. Sun, J.H. Yang, S.Y. Zheng, *J. Colloid Interface Sci.*, 570 (2020) 153.
 12. J. Guo, L.F. Jiao, H.T. Yuan, L.Q. Wang, H.X. Li, M. Zhang, Y.M. Wang, *Electrochim. Acta*, 51 (28) (2006) 6275 .
 13. Y.H. Ding, P. Zhang, Y. Jiang, D.S. Gao, *Solid State Ionics*, 178 (2007) 967.
 14. Y.Y. Hu, Z.Z. Qin, J. Pei, B.W. Cong, X. Yang, J. Chen, *ChemElectroChem*, 7 (2020) 246.
 15. J.F. Zhou, B.C. Zhao, J.Y. Song, B.Z. Chen, X.H. Ma, J.M. Dai, X.B. Zhu, Y.P. Sun, *Solid State Ionics*, 322 (2018) 30.
 16. L.Q. Ban, M. Gao, G.Y. Pang, X.T. Bai, Z. Li, W.D. Zhuang, *J. Mater. Eng.*, 48 (2020) 103.
 17. W.D. Wang, W.H. Qiu, Q.Q. Ding, Nickel cobalt manganese based cathode materials for Li-ion batteries technology production and application, Chemical Industry Press, (2015) Beijing, China.
 18. Y.H. Zhai, P.P. Zhang, J.F. Zhou, Y.P. He, H. Huang, Z.C. Guo, *Mater. Rep.*, 35 (2021) 7056.
 19. G. Farid, G. Murtaza, M. Umair, H.S. Arif, N. Muhammad, M. Ahmad, *Mater. Res. Express*, 5 (2018).
 20. R.Q. Chen, *Trans. Nonferrous Met. Soc. China*, 8 (2021) 107.
 21. C.F. Liao, H.H. Chen, Z.P. Chen, *Nonferrous Met. Sci. Eng.*, 18 (2004) 33.
 22. Y.H. Gui, G.R. Hu, H.Q. Zhao, Q.W. Qin, *Conservation Util Miner Res.*, 4 (2003) 41.
 23. X.H. Liu, L.F. Xiang, J. Gao, M.J. Zhou, *Min Metal Eng.*, 31 (2011) 108.
 24. M.M. Thackeray, S.H. Kang, C.S. Johnson, J.T. Vaughey, R. Benedek, S.A. Hackney, *J. Mater. Chem.*, 17 (30) (2007) 3112.
 25. Y.J. Liu, X.J. F, X Huang, D.M. Liu, A.C. Dou, M.R. Su, D.W. Chu, *J. Power Sources*, 403 (2018) 27.
 26. Y.K. Han, X.J. Shan, G.B. Zhu, Y. Wang, Q.T. Qu, H.H. Zheng, *Electrochim. Acta*, 329 (2020) 135057.
 27. F. Fu, Y.Y. Huang, P. Wu, Y.K. Bu, Y.B. Wang, J.N. Yao, *J. Alloys Compd.*, 618 (2015) 673.
 28. Y.J. Liu, S.Q. Zheng, Q.L. Wang, Y.B. Fu, H.F. Wan, A.C. Dou, V Battaglia, M.R. Su, *Ceram. Int.*, 43 (2017) 8800.
 29. Z.H. Zheng, Q. Li, Introduction to rietveld refinement with X-Ray power diffraction data GSAS software, China Building Materials Press, (2016) Beijing, China.
 30. J. Kikkawa, T. Akita, M. Tabuchi, M. Shikano, K. Tatsumi, M. Kohyama, *Electrochem. Solid-State Lett.*, 11 (11) (2008) A183.
 31. Z.Q. Deng, A. Manthiram, *J. Phys. Chem. C*, 115 (14) (2011) 7097.
 32. M.M. Thackeray, S.H. Kang, C.S. Johnson, J.T. Vaughey, R. Benedek, S.A. Hackney, *J. Mater. Chem.*, 17 (30) (2007) 3112.
 33. J.R. Croy, K.G. Gallagher, M. Balasubramanian, Z.H. Chen, Y Ren, D Kim, S.H. Kang, D.W. Dees, M.M. Thackery, *J. Phys. Chem. C*, 117(13) (2013) 6525.
 34. D. Wang, Y. Huang, Z.Q. Huo, L. Chen, *Electrochim. Acta*, 107 (2013) 461.
 35. D.M. Liu, X.J. Fan, Z.H. Li, T Liu, M.H. Sun, C Qian, M Lin, Y.J. Liu, C.D. Liang, *Nano Energy*, 58 (2019) 786.
 36. Y.J. Liu, Y.Y. Gao, A.C. Dou, *J. Power Sources*, 248 (2014) 679.
 37. X.W. Lai, G.R. Hu, Z.D. Peng, H. Tong, Y. Lu, Y.Z. Wang, X.Y. Qi, Z.C. Xue, Y. Huang, K. Du, *J. Power sources*, 431(2019) 144.
 38. Y.J. Liu, D.M. Liu, H.H. Wu, X.J. Fan, A.C. Dou, Q.B. Zhang, M.R. Su, *ACS Sustainable Chem. Eng.*, 6(2018) 13045.

39. J.H. Li, Z.Q. Liu, Y.F. Wang, R.G. Wang, *J. Alloys Compd.*, 834(2020)155150.

40. J.H. Gao, T Yuan, S Luo, J.F. Ruan, H Sun, J.H. Yang, S.Y. Zheng, *J. Colloid Interface Sci.*, 70(2020) 153

© 2022 The Authors. Published by ESG (www.electrochemsci.org). This article is an open access article distributed under the terms and conditions of the Creative Commons Attribution license (<http://creativecommons.org/licenses/by/4.0/>).